SOCAR Proceedings

Geology, Geophysics & Formation Evaluation

journal home page: http://proceedings.socar.az

STATIC RESERVOIR CHARACTERIZATION AND ROCK TYPING OF CHIRAG RESERVOIR

N. Sh. Aliyev

«OilGasScientificResearchProject» Institute, SOCAR, Baku, Azerbaijan

A B S T R A C T

This study presents the identification and classification of eight distinct petrophysical rock types in the GCA-1 well of the Chirag field using a comprehensive petrophysical integration workflow. The Petrophysical Integration Process Model (PIPM) was applied through two independent yet complementary approaches: the Winland method, supported by capillary pressure data for pore throat radius characterization, and a statistical clustering methodology, including elements from Heubeck and other prior works. Both approaches yielded consistent rock type classifications and leveraged permeability as the primary distinguishing parameter, given its variation across five orders of magnitude and its dominant control on fluid flow behavior. Pittman's R_{20} methodology, which defines the pore throat radius at the 20th percentile mercury saturation, demonstrated the strongest correlation between pore throat size and permeability, making it the most effective tool for rock typing in this dataset. A reasonably strong correlation between porosity and permeability was also observed, providing additional confidence in the classification results. The identified rock types show a general correspondence with depositional lithofacies as defined by Reynolds and Nummedal; however, rock types often transcend individual lithofacies boundaries. This emphasizes the need for integrated petrophysical approaches that go beyond sedimentological classification alone. The integration of multiple datasets and methodologies provides a robust foundation for reservoir characterization and flow unit delineation within a geologically complex and tectonically active setting. The workflow and findings from this study deliver valuable insights for field development planning, reservoir modeling, and future petrophysical evaluations in similar depositional systems.

Keywords: Vychegda Trough; Domanic Formation; hydrocarbon potential; basin modeling; source rock; generation potential.

Date submitted: 17.12.25 **Date accepted:** 14.03.26

Introduction

Chirag rock petrophysics

Efficient field development requires a comprehensive understanding of reservoir rock and fluid properties and their interactions. Rock petrophysics study in combination with formation evaluation and seismic provides the most effective means of assessing reservoir quality, characterizing lithology and rock types, and ultimately to defining flow units, which are of utmost importance in reservoir modeling [1-4]. Proper reservoir characterization, when integrated with a flow simulator, enables effective reservoir management [5-10].

In this article, PIPM process [11-13] is applied by discussing the main part Stage 1:

- Characterization of lithofaies
- Characterization of minerals and clays
- Characterization of rock types

The plug and testing procedure used in this study is according to Gunter [14]

Detailed core studies are conducted on plugs in representative rock intervals. Preliminary plug locations are chosen based on log character and early standard core analysis (SCAL-porosity, permeability, grain density, Dean Stark water saturation, etc.). The selected whole core sections are then fluoroscoped to identify bedding orientation, ensure that plug locations are truly representative of the rock interval, and exclude samples that are affected by local inhomogeneities such as thin clay or heavy mineral laminae, bioturbation, fractures, etc. Individual plugs are drilled parallel or perpendicular to bedding using mineral oil and then cut into segments. Each segment is analyzed using some or all of the following tests: high-pressure mercury injection (HPMI), thin section analysis, porosity & permeability (CMS300), grain density, X-ray diffraction (XRD), FTIR, scanning electron microscope (SEM) analysis, elemental analysis and/or laser particle size. This analysis ensures that each plug is utilized to its fullest potential, core damage is minimal, and tests can cross correlate to verify findings at a single location.

E-mail: nusret.aliyev@socar.az

http://dx.doi.org/10.5510/OGP20260101140

Key findings

- Reynolds [15-17] and Reynolds and Nummedal [18, 19] identified seven lithofacies from a core petrology and sedimentology study. The primary depositional texture (e.g., grain size, shale content, degree and type of lamination) and oil staining (degree of fluorescence) are principal factors used to distinguish lithofacies.
- Stratigraphic variation in reservoir quality for the GCA-1 cores can be expressed as Pereriv B and D intervals > Pereriv A and C intervals > Balakhany X interval.
- Based on petrographic and core analysis data on 17 selected sandstone, siltstone and shale core specimens from the GCA-1 well:
  1. Lithologically, core specimens were grouped as sandstones (14), siltstone (1), and shale (2).
     – Characteristically, the sandstone samples are classified as sublitharenites and, to a lesser extent, litharenites and feldspathic litharenites.
     – Texturally, sandstones vary from lower-fine- to upper-fine-grained and moderately poorly to well-sorted.
     – Mineralogically, detrital mineral constituents account for 69-82 volume percent in sandstone specimens, consisting mainly of quartz, lithic fragments, and feldspar.
  2. Thin section evaluation indicates that sandstones exhibit moderate to excellent reservoir quality with effective matrix porosity in the range of 16.0-28.9 %. These values are reflected in comparable core analysis measurements of 16.0-26.5 % porosity and 0.2-900 mD permeability.
  3. Petrographic evidence suggests that mainly primary textural parameters (sorting and grain size), detrital clay matrix, and physical compaction of ductile lithic grains (mainly shale fragments) control porosity/permeability development in sandstone specimens. Physical compaction accounts for roughly 30-60 % of effective intergranular porosity loss.
- Overall, there is a fairly good correlation between mini-plug-measured permeability and porosity.
- Eight petrophysical rock types are distinguished based on the implementation of the petrophysical integration process model (PIPM) by applying two methods:
  1. Winland pore throat radius characterization, followed by confirmation with capillary pressure pore throat radius characterization [20]
  2. Statistical approach (Doveton 1998 and Heubeck 1999) [21, 22]. Both methods identify consistent rock types and use permeability to distinguish different rock types since permeability changes over five log cycles and controls the flow.
- Pittman R_{20} (the pore throat radius corresponding to the 20th percentile mercury saturation) lines of constant pore aperture yield the best overall correlation coefficient for all rock types identified in this study for the GCA-1 cores.

High-pressure mercury injection data corroborate the classified rock types.

An overall good correlation was obtained between depositional lithofacies (as defined by Reynolds and Nummedal [19]) and identified rock types.

Upper (A & B), middle (C) and lower (D) good-quality Pereriv sands are dominated by rock types 1-5 (lithofacies 1-5) and upper and lower Pereriv shales and Balakhany X zones by rock types 2-7 (lithofacies 2-7).

Ambient porosity and permeability measurements (400 psi and 77°F) overestimate these properties at reservoir conditions (4500 psi and 150°F) by 5-8% for porosity and 12-14 % for permeability.

Methodology

Petrophysical integration process model

Figure 1 is a process map for integrating geology, engineering, and geophysics developed by the team leaders of the Amoco Petrophysics Training Program [11-13, 23]. This process map leads to a quality description of a reservoir, regardless of geology setting, hydrocarbon type, maturity, or

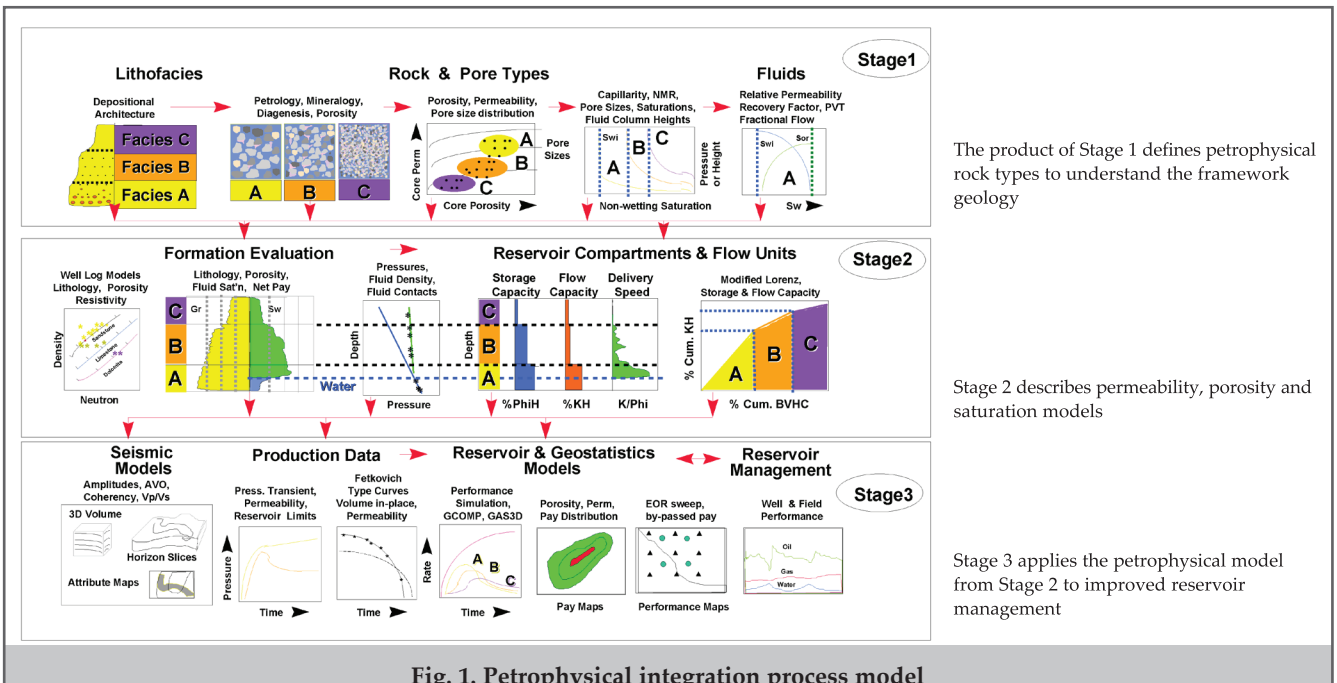

The product of Stage 1 defines petrophysical rock types to understand the framework geology

Stage 2 describes permeability, porosity and saturation models

Stage 3 applies the petrophysical model from Stage 2 to improved reservoir management

Fig. 1. Petrophysical integration process model

location. Integration of all forms of data maximizes understanding of the controls on hydrocarbon production [5, 6]. This approach was applied to the analysis of the Chirag reservoir within the GCA megastructure.

Lithofacies analysis of the GCA-1 cores

Depositional systems are composed of units of rock-termed lithofacies. A lithofacies is a three-dimensional mass of sedimentary rock distinguishable from adjacent rock units based on its lithology, texture, geometry and sedimentary structure. Reynolds and Nummedal [15-19] previously conducted lithofacies analysis of the GCA-1 cores. Seven distinct lithofacies characterize the depositional environment:

1. Facies 1 (6.2% of the total GCA1 cores) - Interclast conglomerate in a sandstone matrix; sandstone ranges from upper fine to lower medium grain size.
2. Facies 2 (21.3%) - Moderate brown, mostly fine-grained sandstone. Internally distinguished by cross-bedded, rippled, low-angle to horizontal laminated or massive sublithofacies.
3. Facies 3 (7.6%) - Pale brown sandstone, very similar to Facies 2. Contains all Facies 2 sublithofacies except the massive.
4. Facies 4 (20%) - Brown, mostly fine-grained sandstone with blue-gray laminations. Internally consists of rippled, low-angle to horizontal laminated or massive sublithofacies.
5. Facies 5 (17.8%) - Blue-gray sand and silt with brown laminations. Combines very fine sand, silt (grain size range 30 -60 microns) and tiny mud aggregates in cross-bedded, rippled and low-angle to horizontal laminated sublithofacies.
6. Facies 6 (10.5%) - Gray and brown silt without sand; rippled, low-angle to horizontal laminated sublithofacies.
7. Facies 7 (13.6%) - Massive and laminated mudstones; dark blue-gray or gray massive or laminated mudstone sublithofasies.

Six intervals described as lower Pereriv (D) sandstone (2845.8-2871.4 meters), lower shale (2839.5-2845.8 m), middle Pereriv (C) sandstone (2816.5-2839.5 m), upper shale (2807-2816.5 m), upper Pereriv (B) sandstone (2772-2807 m) and Balakhany X sandstone (2662-2714 m).

A 3D facies distribution plot (figure 2) illustrates the spatial relationship between lithofacies and stratigraphic units. The analysis shows that the highest-quality lithofacies (1–5) are concentrated in the Upper and Lower Pereriv sandstones, followed by the Middle Pereriv and Balakhany X sandstones. Lithofacies 6 and 7, which represent lower-quality facies in terms of reservoir potential, are dominant in the Upper and Lower shale zones and more sporadically present in the Balakhany X interval.

Mineralogy of the GCA-1 cores

Total mineralogy is particularly important for log response prediction and nuclear modeling (NMOD) for porosity determination, while clay mineralogy is important for the calculation of water saturation from logs. Three techniques are used to quantify mineralogy for the GCA-1 cores: (a) thin section model analysis and point counting (TS); (b) X-ray diffraction; and Fourier transform infrared spectroscopy (FTIR). Scanning electron microscopy (SEM) provides additional mineralogical information. Each of these mineralogical analytical techniques has strengths and limitations [5]:

Thin-section point-count analysis can reliably determine texture and identify and quantify the most abundant minerals, particularly in grains greater than silt size. One can also make conclusions regarding origin, for example, detrital versus authogenic. However, this method is poor at quantifying low abundance minerals and at identifying clay minerals.

X-ray diffraction provides a rapid analysis of bulk mineralogy without determining its origin. Fine fraction (<2 microns) analysis can accurately identify clay mineral types but is relatively poor at quantifying their absolute abundance. The disaggregation process in sample preparation can release fine fragments from clay clasts to an unknown degree, and clay flocculation in the settling column may lose clay minerals from the fine fraction [24]. In addition, most kaolinite and some crystals are larger than 2 microns and therefore may be underestimated.

Fourier transform infra-red spectroscopy provides a rapid bulk quantification of the 15 minerals analyzed for, though the technique is poor at identifying and quantifying clay minerals [14] due to overlapping spectra and, therefore, nonunique inversion.

Scanning electron microscopy is useful for determining texture, clay mineral type and habit, and the paragenetic sequence. In addition, energy dispersive spectroscopy (EDS) can make pinpoint chemical analyses of chosen grains or crystals. The technique is of little use in quantifying mineral abundance.

Independent measurements of sandstone composition, such as routine core analysis (RCAL), grain density and SEM clay mineral identification, can reconcile some of these differences and establish likely average sandstone mineralogy.

Sandstone classification bulk mineralogy

X-ray diffraction and Fourier Transform Infrared Spectroscopy are used for mineralogy profiling of GCA-1 well cores. FTIR has problems distinguishing between clay minerals and carbonate minerals. Thus, in this section results of XRD data is illustrated.

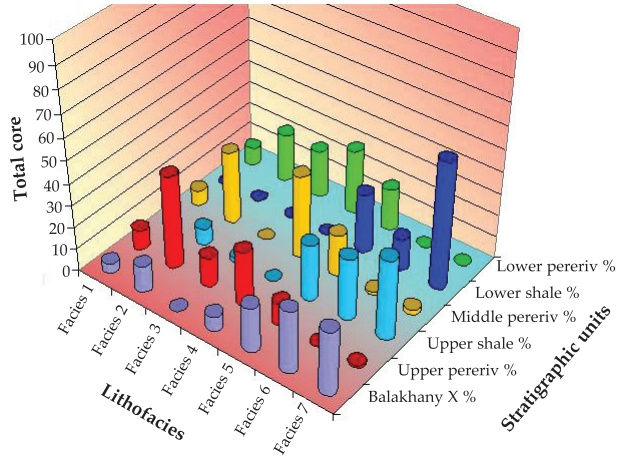

Indicates that lithofacies 1-5 occur mostly in Pereriv sand intervals, whereas lithofacies 6 and 7 mainly occur in shale and Balakhany X intervals

Fig. 2. 3D Cross-Plot of Lithofacies and Stratigraphic Units for the GCA-1 Core

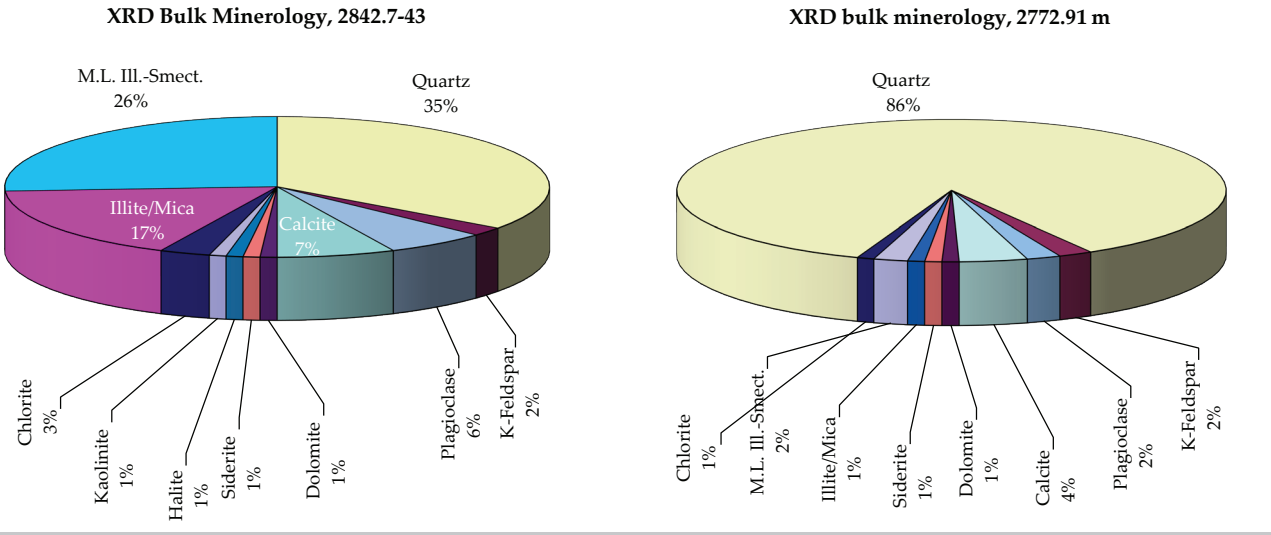

Fig. 3. Total mineralogy pie plot for the Pereriv sands

Fluvial-dominated sediments are rich with quartz minerals (70-90 %), and X-ray diffraction mineralogy data indicate that clay mineral content increases as the depositional energy decreases. Except for an extremely quartz-rich sample, the Pereriv Sands exebit a relatively constant feldspar composition (≅2%). Variation in mineralogy are primarily controlled by changes in the relative proportions of quartz and clay minerals, illite/mica and ML illite-smectite (fig. 3). Minor amounts of dolomite, siderite and halite account for the remaining lithic fraction as well. A detailed sandstone classification is provided by Folk [25].

Rock types cannot be distinguished by mineralogy alone; however, it remains a key component of rock typing and should be incorporated into its determination. In the Pereriv sands, mineralogical variation is primarily controlled by changes in the relative proportions of quartz and lithic fragments.

Clay mineralogy

Clays in these sands represent original detrital sediment, and there is a strong correlation between depositional environment and lithic content.

Figure 4 shows the X-ray diffraction clay mineralogy distribution for Pereriv sands. Calcite is the predominant cement in these sands, with minor amounts of dolomite and siderite found from the carbonate fragments.

Values are in weight percent. Laminated clay is dominant (50 and 56 % M.L.IIlite-Smectite) in the Upper and Lower Pererive interval. XRD data indicates mainly trace amounts of Kaolinite mineral across all Pereriv sands.

Laminated clay and structural clay are the two dominant types, representing 80-90 % of the total clay volume. Laminated clay predominates in the Upper and Lower Pereriv and Balakhany shales, and structural clay is dominant type in the Pereriv and Balakhany Sands.

Rock type characterization

Rock typing is defined as «a unit of rock deposited under similar conditions which experienced similar diagenetic processes resulting in a unique porosity-permeability relationship, capillary pressure profile and water saturation for a given height above free water in a reservoir» [12].

Porosity and permeability are the properties that give determine reservoir's capability, its ability to storage and

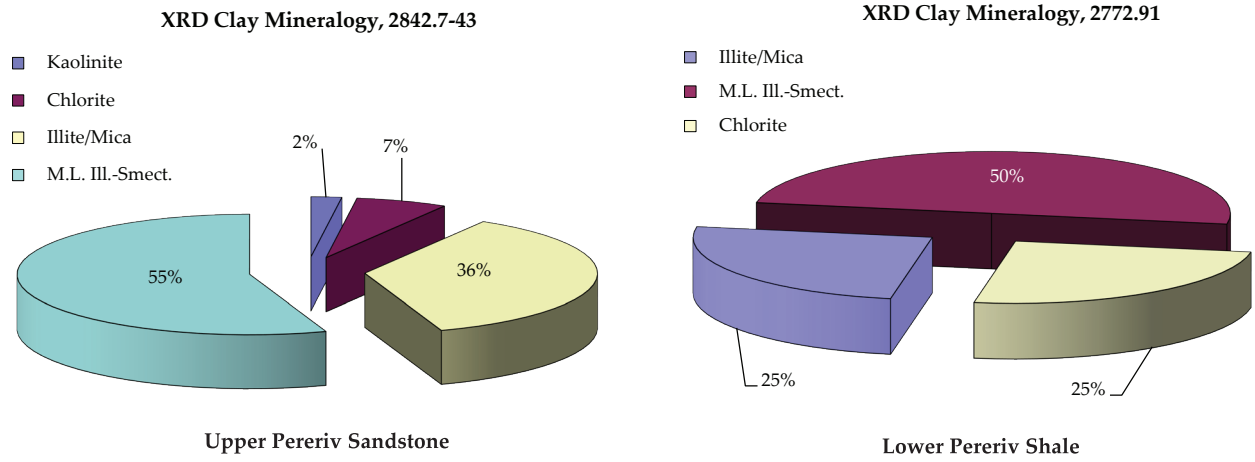

Fig. 4. Example composition of lithic mineralogy fraction from XRD for different sands

transmit fluids). These properties are controlled by depositional processes, and thus their prediction is based on analysis and identification of rock types. The rock type analysis is accomplished through continued data integration, including:

- Direct evidence derived from observation of rocks (lithofacies analysis, mineralogy, outcrops analysis, well cuttings and cores),
- Indirect evidence (data recorded by wireline logs and seismic sections),
- Production data, interwell log correlations and detailed mapping.

In fact, the rock type analysis bridges the gap between the static reservoir characterization, which is accomplished through petrology and sedimentology (lithofacies analysis and mineralogy) and dynamic reservoir characterization (production). The rock type analysis ultimately defines flow units, which are critical input into a flow simulator to be used for a realistic forecast of rate and recovery for a given field [5, 7, 8]

One must recognize that the rock type analysis should be continuously updated and reinterpreted as a reservoir matures through continued drilling and subsurface data accumulation. New analyses may result in the discovery of new reserves or even new reservoirs.

Rock types are identified using the following procedure:

1. Distinguish rock types based on the core porosity and permeability relationship.
2. Validate step 1 using «Winland or Pittman» pore throat radii distributions.
3. Confirm rock types by high-pressure mercury injection capillary pressure curve character and calculated dominant pore throat radii.
4. Identify rock types using a statistical approach.
5. Explain rock type properties through integration with lithology and mineralogy.

Porosity and permeability

A large number of porosity and permeability plug measurements are available for GCA-1 well. Most of these measurements were done by AZLAB in Baku, while the PTS Lab in Houston performed additional measurements for Amoco over several years. All measurements were carried out at ambient temperature and confining pressures of 400 and 500 psi.

Figure 5 shows a good correlation between permeability (k) and porosity (φ) plotted on a semilog scale. The line represents the power-function regression of the data, yielding a correlation coefficient of 0.73, which indicates a reasonably good relationship between k and φ.

Winland pore throat radius characterization

Pore throat radius distribution determines fluid flow and capillary forces in the reservoir and has been characterized by two methods:

1. From RCAL porosity and permeability data (at ambient conditions) using a Winland relationship, and
2. From high-pressure mercury injection capillary pressure data.

Winland [20] defined a representative pore throat radius based on an empirical correlation between porosity and permeability at ambient conditions and pore-throat radius from mercury injection capillary pressure tests:

$$Log(R_{35}) = 0.732 + 0.588 \cdot Log(k) - 0.864 \cdot Log(\varphi) \qquad (1)$$

Where R35 is the pore aperture radius corresponding to the 35th percentile mercury saturation. Pittman later modified Winland's equation and proposed a similar empirical equation with different constants:

$$Log(R_{35}) = 0.255 + 0.565 \cdot Log(k) - 0.523 \cdot Log(\varphi) \qquad (2)$$

Lines of equal-R35 pore throat radius divide the RCAL data from the GCA-1 well into seven rock types, as shown in figure 6:

1. An excellent reservoir-quality group (rock types 1-3) with pore throat radius greater than 5 micron and permeability greater than 100 mD,
2. A good reservoir quality group (rock types 4 and 5) with pore throat radius of 1-5 microns and permeability in the range of 10-100 mD,
3. A low reservoir quality group (rock type 6) with pore radius of 0.5-1 micron and permeability in the range of 1-10 mD, and
4. A very low reservoir quality reservoir group (rock type 7) with pore throat radius of less than 0.5 micron and permeability less than 1 mD.

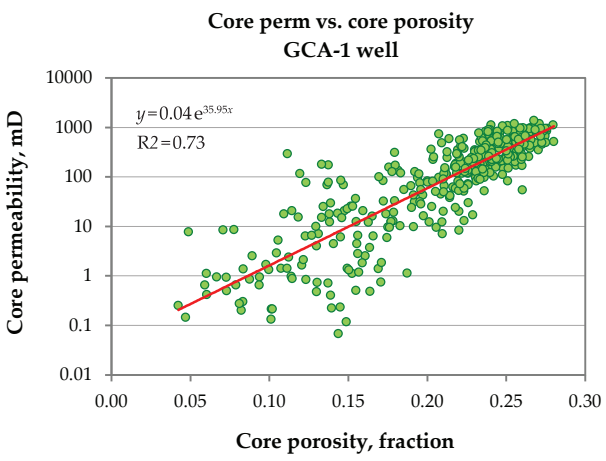

Fig. 5. Semilog plot of core measured permeability vs porosity

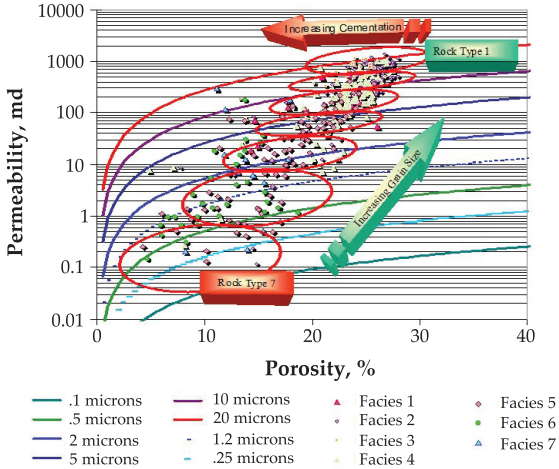

Fig. 6. Rock type designation from porosity and permeability data

Capillary pressure pore throat radius characterization

Capillary pressure estimates the resistance of a wetting phase (in this case, water) being displaced by a non-wetting phase. The size and distribution of pore throats, degree of sorting, and hydrocarbon column heights are qualitative and quantitative parameters derived from capillary pressure curves.

The standard equation for determining capillary pressure is:

$$P_c = \frac{2 \cdot \sigma \cdot \cos(\theta)}{r} C \qquad (3)$$

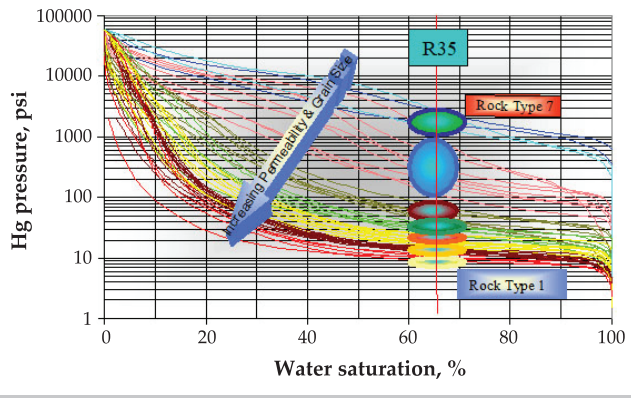

Fig. 7. Rock type designation from 38 capillary pressure curves (ambient condition)

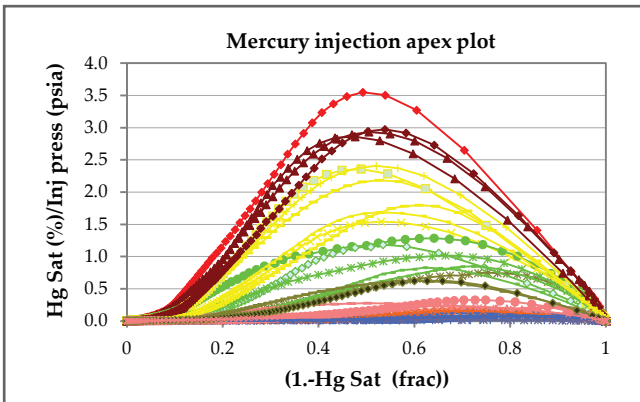

Fig. 8. Rock type designation from apex plots

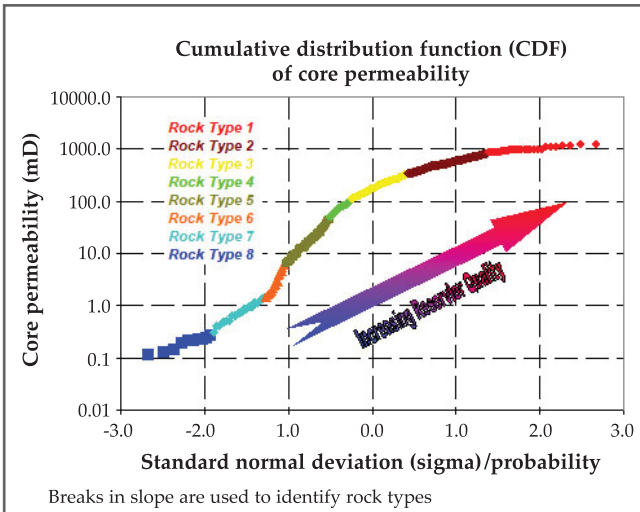

Fig. 9. Rock type designation from permeability CDF

where P_c is the capillary pressure in psia; σ is the interfacial tension between air and mercury (480 dynes/cm); θ is the mercury contact angle in air (140 degrees); r is the pore throat radius in microns; and C is a conversion factor (145×10^{-3}).

The lines on the chart represent constant pore throat radius, calculated using Equation (2), the modified Winland R_{35} equation.

High-pressure mercury injection data provide information on pore throat radii distributions, as the capillary pressure required to inject mercury into a pore network is controlled primarily by the pore throats rather than the pore bodies. The dominant pore throat radius and dominant saturation can be derived from apex plots; see Thomeer [26], Swanson [3], and Pittman [27]. The dominant pore radius obtained from the apex plot represents the radius of the interconnected pore throat population that controls fluid flow [27]. The dominant saturation is the saturation at which the dominant pore throat population is filled. Pore throat characterization from capillary pressure and apex plots for the GCA-1 core plugs is presented in figure 7 and figure 8, respectively. As shown in figure 7, bimodality in the pore throat radii distributions is evident for lower quality rock types 6 and 7.

The apex plot describes the effective pore throat network distribution and the dominant pore radius. For the GCA-1 plugs, the dominant apex saturation ranges from 10% (poor-quality reservoir rock, seal) to 50% (excellent reservoir quality). Higher apex values correspond to lower entry pressures and a more extensive interconnected pore throat network.

Statistical approach for rock typing

The approach used in this study combines the methods of Doveton [21] and Heubeck [22]. The procedure includes the following steps:

1. Generate cumulative distribution functions (CDFs) for variables of interest (e.g., core permeability, porosity or k/φ) under the assumption of normal distribution. The goal is to select a variable that shows distinct separation when the rock types.
2. Classify rock types by plotting the CDF of the selected variable and identifying breaks in slope, assuming normal distribution.
3. Determine pore throat radii using one of Pittman's equations, selecting the equation that yields the best overall correlation coefficient across all rock types.
4. Validate the classification by by comparing the rock types identified with this method to those obtained previously.

After examining CDF plots of porosity, permeability, and k/φ, a permeability range was selected for rock type identification. Both porosity and k/φ CDFs exhibit difficulties at the very low and very high ends of their distributions. Figure 9 illustrates rock type classification using the permeability CDF plot. Most measured data fall within two standard deviations. Rock types 1–6 are consistent with the rock types 1–6 identified by the previous method (Winland permeability–porosity method). The only difference occurs at low permeability values, where rock type 7 from the previous method is subdivided into rock types 7 and 8 in the present approach.

Figure 10 depicts the frequency and cumulative plots of permeability distribution versus permeability values (permeability histogram). The median occurs at a permeability of 176

mD in the rock type 3, indicating 50% of samples have permeability larger than 176 mD (and belong to rock types 1-3).

Figure 11 and figure 12 show permeability and porosity cumulative plots versus permeability and porosity, respectively. Clearly, porosity overlaps for several rock types, especially at the low and high ends of the values. In contrast, the permeability plot (figure 11) shows clear separation between all rock types, with no overlap.

Porosity values overlap among rock types, making it less suitable for rock type identification in the GCA-1 system.

Finally, the best match of permeability-porosity data associated with the identified rock types was obtained using the Pittman R_{20} method, (where R_{20} is the pore aperture radius corresponding to the 20th percentile mercury saturation), according to the following equation:

$$Log(R_{20}) = 0.218 + 0.519 \cdot Log(k) - 0.303 \cdot Log(\varphi) \quad (4)$$

Figure 13 illustrates the Pittman R_{20} porosity-permeability plot. The lines were calculated to provide the best fit for each rock type using Equation (4) by adjusting the pore throat radius.

Finally, table summarizes of rock type properties, including permeability, porosity and pore throat radius.

Integration of rock types, lithology and mineralogy

So far, eight rock types have been identified from the GCA-1 cores. In the next two sections of this study, the PIPM process presents the results of formation evaluation and the integration of rock types, formation evaluation, and reservoir engineering to providing a comprehensive reservoir characterization for effective reservoir management of the Chirag field.

Since rock typing bridges the gap between static measurements (such as lithology and mineralogy) and dynamic reservoir behavior (such as production), it is essential to establish a strong correlation between rock types and lithofacies analysis.

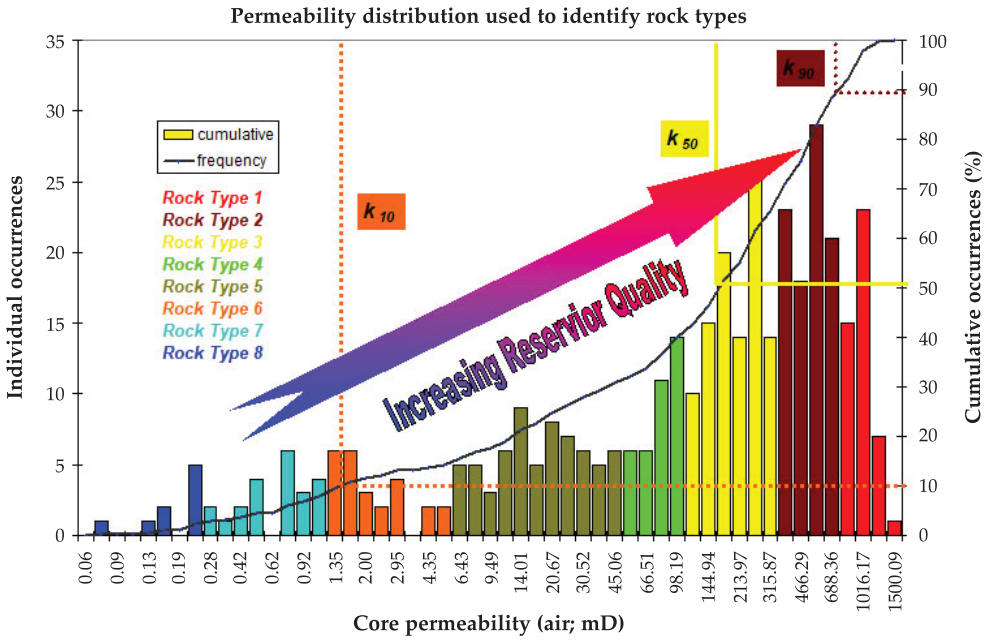

Note that the sample population for rock types 2, 3 and 5 is significantly higher

Fig. 10. Rock type designation from CDF of core permeability

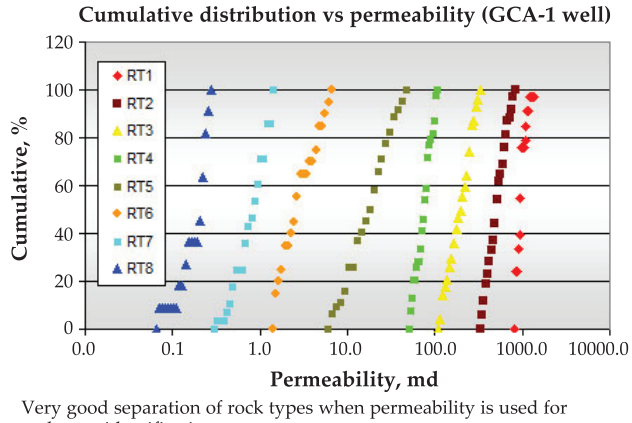

Very good separation of rock types when permeability is used for rock type identification

Fig. 11. Cumulative distribution of permeability vs. permeability for all rock types

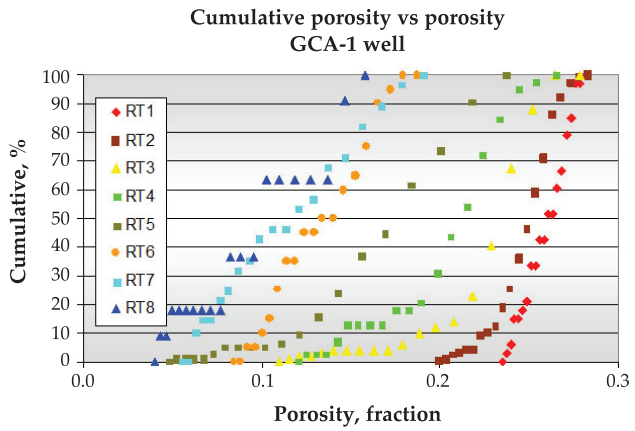

Fig. 12. Cumulative distribution of porosity vs porosity for all rock types

Table

Rock type summary

Rock type	Porosity, frac.			Permeability, md			Pore size, micron		Lithofacies present
	φ_{10}	φ_{50}	φ_{90}	k_{10}	k_{50}	k_{90}	dominant	Pittman R_{20}	
1	0.240	0.260	0.275	830.00	950.00	1140.00	> 9	20.0 – 25.0	F2-F4
2	0.227	0.251	0.260	350.00	500.00	738.00	7.0 – 9.0	12.5 – 20.0	F1–F4 and F5*
3	0.190	0.231	0.258	120.00	197.00	289.00	5.0 – 6.5	7.50 – 12.5	F1-F5 and F6* and F7*
4	0.144	0.210	0.238	53.00	75.00	98.00	3.0 – 7.0	5.00 – 7.50	F1–F5
5	0.121	0.170	0.217	7.85	17.80	38.00	1.7 – 4.0	1.80 – 5.00	F1–F2, F4–F5 and F6* and F7*
6	0.100	0.134	0.165	1.45	2.59	5.60	0.50 – 1.0	1.00 – 1.80	F5-F7
7	0.062	0.119	0.174	0.44	0.84	1.35	0.07 – 0.50	0.500 – 1.00	F5-F7 and F4*
8	0.046	0.098	0.146	0.11	0.22	0.26	> 0.07	0.180 – 0.500	F5-F7 and F4*

Parameters in table 1 is based on RCAL measurements on mini-plugs from the GCA-1 core under ambient conditions. The asterisk (*) indicates a small sample population

Based on integration of rock typing, lithology (depositional character), and mineralogy (textural characteristics), the primary factors controlling rock types are identified as:

1. Grain size – finer-grained rocks generally exhibit lower porosity and permeability.
2. Detrital clay – cleaner rocks tend to have higher porosity and permeability.
3. Grain sorting – better sorting enhances both porosity and permeability.
4. Compaction – has a negative impact on porosity and permeability.

Overall, there is a reasonably good correlation between depositional lithofacies and the identified rock types.

Figure 14 illustrates the relationships between the depositional lithofacies and the rock types for GCA-1 core samples. Variation of lithofacies within rock types shows that:

- Lithofacies 2 and 3 are predominantly composed of rock types 1-3, consistent with the intense fluorescence of Facies 2 and 3 cores, indicating high oil saturation. Facies 1, being a conglomerate, exhibits wide scatter in porosity and permeability at the plug scale.
- Rock types 1-3 (57.4% of plugged cores) are composed of Lithofacies 1-4.
- Lithofacies 4 is approximately 71.8% very good reservoir rock (rock types 1-3), 21.8% intermediate reservoir rock (rock types 4 and 5) and 7.4% poor or non-reservoir rock (rock types 6 and 7). This alignes with its lower-energy depositional environment and less intense fluorescence compared to Lithofacies 1-3.
- Lithofacies 2 and 4 are the predominant components of rock types 1-3.
- Rock types 4 and 5 (23.7% of total plugs) represent a transition from good reservoir-quality rocks (lithofacies 1-5) to poor reservoir-quality rocks (lithofacies 6 and 7) and predominantly consist of Lithofaces 4 and 5.
- Lithofacies 5 ranges over the whole range of rock types, but it is dominantly lower quality reservoir rock or non-reservoir rock (70.1% is rock types 5-7). This is consistent with its low-energy depositional environment and its low level of core fluorescence.
- Lithofacies 5 and 6 (10% of total plugs) are predominantly rock types 6-8 (18.9%) and represent poor reservoir-quality rocks.
- Lithofacies 7 (3% of total facies) is mainly found in rock types 5-8.

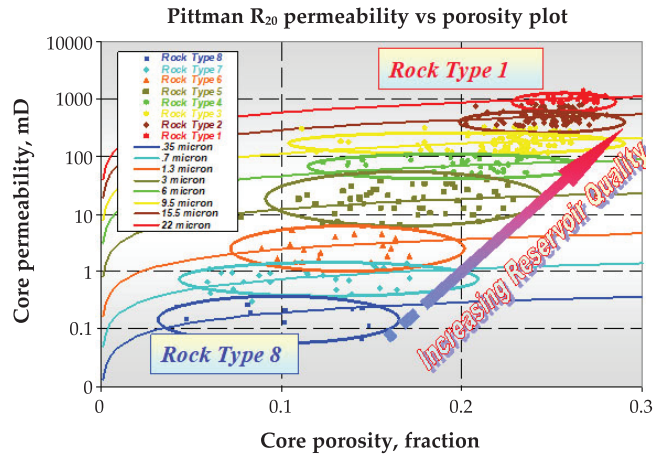

Fig. 13. The Pittman R_{20} porosity-permeability plot

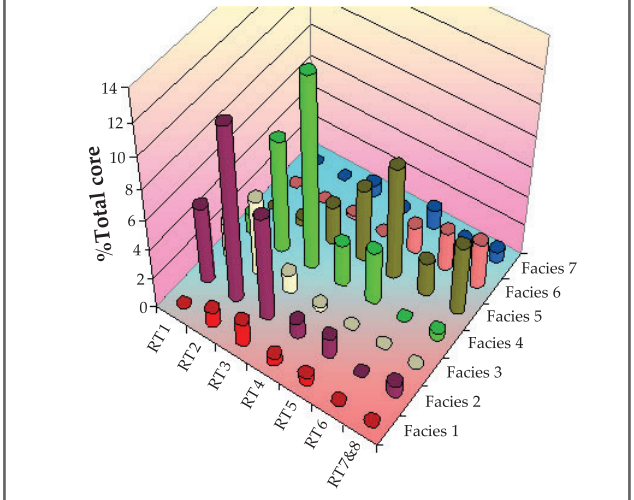

Fig. 14. 3D cross-plot of depositional lithofacies and rock types

Next, each rock type is discussed based on integration with lithofacies and mineralogy.

Rock type 1

Rock type 1 exhibits the highest reservoir quality, capable of producing at high flow rates, and is characterized by a very early water breakthrough time. It consists of clean, massive, poorly consolidated sub-litharenite sandstone.

Sands associated with this rock type are moderately well to well-sorted, upper fine-grained and sub-rounded, indicating high-energy turbidite deposition associated with channel deposits. The dominant pore throat radius exceeds 9 microns, with porosity ranging from 25 to 28 % and very high permeability of 800 mD and higher. High-pressure mercury injection (HPMI) capillary pressure indicates very low entry pressures and a uniform pore throat distribution. Thin section photomicrograph reveals that the framework grains are largely quartz (>85%), with minor amounts of feldspar and shale, chert and carbonate sedimentary rock fragments. Intergranular pores appear well-connected (77%). Cementation and saturation exponents correspondingly are about m=1.65 and n=1.8, while irreducible water saturation is relatively low.

Rock type 2

Rock type 2 has a very good reservoir quality. It consist of massive, laminated and moderate to poorly consolidated litharenite sandstone. These sandstones are medium to lower grained and moderately well sorted, reflecting high-energy deposition within channelized environments.

The dominant pore throat radius exceeds 7 microns, with porosity ranging from 23 to 28 % and permeability between 300 to 800 mD. This rock type is characterized by very low HPMI entry pressures and a uniform pore throat distribution. Thin section and FTIR analyses indicate that the framework composed of 65% quartz with minor amounts of feldspar and other sedimentary rock fragments. Clays are mainly detrital illite and smectite. Intergranular pores are well connected. Cementation, saturation exponents and irreducible water saturation values are similar to those of rock type 1. Compared to rock type 1, rock type 2 exhibits more grain fracturing.

Rock type 3

Rock type 3 is characterized with good reservoir quality. It consist of massive, rippled and laminated, medium-grained litharenite sandstone that is moderately to poorly sorted and associated with channel deposits.

The dominant pore throat radius is higher than 5 microns with a porosity ranging from 22 to 27.5 % and permeability bwteen 100 mD to 300 mD. Thin section and FTIR indicate that framework grains are predominantly consist of quartz, with relatively minor amounts of feldspar and rock fragments. No significant amount of clay minerals was noted. Compared to rock type 2, this rock type exhibits significantly more grain fracturing, poorer sorting, and a wider range of pore throat sizes at a given pressure. Intergranular pores are well-connected. Cementation and saturation exponents, as well as irreducible water saturation, are relatively higher than those of rock type 2.

Rock type 4

This rock type has intermediate reservoir quality. It typically occurs in fining-upward sequences of fine-grained sandstone and horizontally laminated, very fine-grained sandstone. Porosity ranges from 20 to 24 %, with reduced permeability between 50 mD and 130 mD. Although its mineralogy is similar to that of rock type 3, detrital illite is present within the cored interval. The parallel and ripple-laminated character reflects a lower-energy, planar flow regime typical of proximal levee deposits and late-stage channel deposition. The intermediate reservoir quality is mainly due to finer grain size and increased clay content.

Rock type 5

This rock type has low reservoir quality. It is associated with horizontal to ripple-laminated, thin-bedded sandstone and laminated silty claystone. The relatively low porosity (18.0-20.0 %) and permeability (5-60 mD) result from the fine grain size, abundant ductile shale fragments, and high abundance of detrital laminar illite. Clay laminations significantly reduce vertical reservoir communication and may cause flow restriction due to mobilization of illite fines.

Rock type 6

The rock type 6 exhibits a low reservoir quality, occurring over a wide range of lower energy depositional facies and made up of non-fluorescent siltstone and shale sediments, resulting from a variety of sedimentological, petrographical factors.

Porosity is raging from a range of (10-18.0 %) and permeability (3-10 mD) result from the very fine grain size, abundant ductile shale fragments, and high content of detrital laminar illite. Clay laminations significantly reduce vertical reservoir communication and may cause flow restriction due to mobilization of illite fines.

Rock types 7 and 8

Rock types 7 and 8 exhibit the lowest reservoir quality, occurring over a wide range of lower energy depositional facies and made up of non-fluorescent siltstone and shale sediments, from a wide variety of sedimentological, petrographical causes.

Conclusions

- Identified seven lithofacies from a core petrology and sedimentalogy study that has distinct primary depositional and oil staining are principal factors used to distinguish lithofacies.
- Based on petrographic and core analysis of the selected sandstone, siltstone and shale core speciments from the GCA-1 well Lithologically, core specimens grouped as sandstones, siltstone, and shale.
- Fairly good correlation between mini-plug-measured permeability and porosity.
- Eight petrophysical rock types are distinguished based on implementation of the petrophysical integration process model (PIPM) by applying two methods; Winland pore throat radius characterization, followed by confirmation with capillary pressure pore throat radius characterization and Statistical approach
- Pittman R_{20} (the pore throat radius corresponding to the 20^{th} percentile mercury saturation) lines of constant pore aperture yields the best overall correlation coefficient for all rock types identified in this study for the GCA-1 cores.
- Ambient porosity and permeability measurements (400 psi and 77o F) overestimate these properties at reservoir condition (4500 psi and 150°F) by 5-8 % for porosity and 12-14 % for permeability and corresponding adjustments are required incorporating net mean stress.

References

1. Rodriguez, E., Mezzatesta, A., Telzlaff, D. (1989). Determination of statistical confidence interval for petrophysical formation properties. In: *SPWLA, LASER Symposium for Log Analysis Software and Review, December 13-15, London, England.*

2. Smart, C. R., Gunter, G. W., Finneran, J. M., Miller, M. A. (1999). Saturation modeling at the well log scale using petrophysical rock types and a classic non-resistivity based method. In: *The SPWLA 40th Annual Logging Symposium, Oslo, Norway, May.*

3. Swanson, B. F. (1998). A simple correlation between permeabiliies and mercurry capillary pressure. *SPE JPT*, 33(12), 2498-2504.

4. Ti, G., Ogbe, D. O., Munty, W., Hatzignatiou, D. G. (1995). Use of flow units as a tool for reservoir description: A case study. *SPE Formation Evaluation*, 10(02), 122-128.

5. Aliyev, N. Sh., Negahban, Sh. (2000). Petrophysical characterization and reservoir modeling of GSA fields. In: *AAPG Regional International Conference, July 9-12, Istanbul, Turkey.*

6. Adams, C., Gousseinov, B. (1994). Petrophysical characterization of Middle Pliocene reservoirs, Guneshli field, Caspian Sea, Azerbaijan. Report No.: S94-G-01, July 22.

7. Amaefule, J. O., Altunbay, M., Tiab, D., et al. (1993). Enhanced reservoir description: using core and log data to identify hydraulic (flow) units and predict permeability in uncored intervals/wells. SPE-26436-MS. In: *The SPE Annual Technical Conference and Exhibition, Houston, Texas, October.*

8. Brain, G., Aliyev, N. (2012). Simulation modelling of Chirag field water cut. In: *«Khazarneftgazyatag–2012» Scientific – Practical Conference, Baku, Azerbaijan.*

9. Choi, K., Jackson, M. D., Hampson, G. J., et al. (2007). Impact of heterogeneity on flow in fluvial-deltaic reservoirs: implications for the Giant ACG field, South Caspian Basin. In: *The EUROPEC/EAGE Conference and Exhibition, June, London, U.K.*

10. Devlin, W. J., Cogswell, J. M., Gaskins, G. M., et al. (1999). South Caspian Basin: young, cool, and full of promise. *GSA Today*, July, 9(7), 1-9.

11. Gunter, G. W., Pinch, J. J., Finneran, J. M., Bryant, W. T. (1997). Overview of an integrated process model to develop petrophysical based reservoir descriptions. SPE-38748-MS. In: *The SPE Annual Technical Conference and Exhibition, San Antonio, Texas, October.*

12. Gunter, G. W., Finneran, J. M., Hartmann, D. J., Miller, J. D. (1997). Early determination of reservoir flow units using an integrated petrophysical method. SPE-38679-MS. In: *The SPE Annual Technical Conference and Exhibition, October, San Antonio, Texas.*

13. Gunter, G. W., Sahar, M. Y., Allen, D. F., et al. (2021). Integrating rock typing methods including empirical, deterministic, statistical, probabilistic, predictive techniques and new applications for practical reservoir characterization. In: *The Abu Dhabi International Petroleum Exhibition & Conference, Abu Dhabi, UAE, November.*

14. Guest, K. (1990). The use of core-derived quantitative mineralogical data to improve formation evaluation /in: Worthington, P.P. (Ed.). Advances in core evaluation, accuracy, and precision in reserves estimation. *New York: Gordon and Breach.*

15. Reynolds, A. D., Simmons, M. D., Bowman, M. B. J., et al. (1998). Implications of outcrop geology for reservoirs in the Neogene Productive Series: Absheron Peninsula, Azerbaijan. *AAPG Bulletin*, 82, 25-49.

16. Reynolds, A. D. (2006). The geological use of pressure data: examples from the development of the Giant ACG oil field, Azerbaijan. In: *The Abu Dhabi International Petroleum Exhibition and Conference, November, Abu Dhabi, UAE.*

17. Reynolds, A. G. (1997). GCA1 reservoir quality study. September.

18. Nummedal, D. (2002). The hydrocarbons of the South Caspian Basin: How exploitation depends on the understanding of Neogene Paleoclimate. In: *AAPG Annual Meeting, March 10-13, Houston, Texas.*

19. Reynolds, A. J., Nummedal, D. (1997). GCA1 core description study. September 16.

20. Winland, H. D. (1972). Oil accumulation in response to pore size changes. Amoco Production Research Report, No. F72-G-25, Saskatchewan.

21. Doveton, J. H. (1998-1999). Short course on basic statistics for petrophysicists.

22. Heubeck, C., Gunter, G., Smart, C. (2000). Integrated reservoir characterization of the Fulmar Formation in the Appleton and Halley Complexes, UK North Sea: An analog for Eastern Canada offshore fields. In: *GeoCanada 2000 (Joint Annual Meeting GAC, MAC, CSPG, SPWLA), May 29-June 2, Calgary.*

23. Gunter, G. W., Sigal, R. F. (1997). Gunashli-Chirag-Azeri (GCA) GCA Well No. 1 Caspian Sea, Azerbaijan Core Study. July.

24. Emery, D., Robinson, A. (1993). Inorganic geochemistry: applications to petroleum geology. *Blackwell Scientific Publications.*

25. Folk, R. L. (1974). The petrology of sedimentary rocks. *Austin: Hemphill Publishing Co.*

26. Thomeer, J. H. M. (1960). Introduction of a pore geometrical factor defined by the capillary pressure curve. *SPE JPT*, 12(03), 73-77.

27. Pittman, E. D. (1992). Relationship of porosity and permeability to various parameters derived from mercury injection capillary pressure curves for sandstones. *AAPG Bulletin*, 76(2), 191-198.